1D SiC decoration of SiC macroscopic shapes for filtration devices†

Estelle Vanhaecke,[a] Svetlana Ivanova,[a] Adrien Deneuve,[a] Ovidiu Ersen,[b] David Edouard,[a] Gauthier Winé,[a] Patrick Nguyen,[c] Charlotte Pham[c] and Cuong Pham-Huu*[a]

Received 22nd April 2008, Accepted 4th July 2008
First published as an Advance Article on the web 22nd August 2008
DOI: 10.1039/b806785f

The synthesis of a hierarchical support, constituted of a network of SiC nanofibers deposited on a SiC foam host resulting in a ceramic material with a controlled macroscopic shape and associated high specific surface area superior to 50 $m^2\ g^{-1}$, has been reported for the first time. The new composite combines the nanoscopic properties of the SiC nanofibers' network and controlled macroscopic shape and open porosity, typical of a SiC foam structure. The introduction of the nanostructures onto the host material allows a dramatic increase in the effective surface area which is extremely useful for the chosen field of application. This new type of material has been efficiently employed as a diesel particulate filter at high space velocity and without a detrimental pressure drop. In addition, the combination of such a hierarchical structure with high thermal conductivity could give rise to unexpected results in the field of heterogeneous catalysis where the mass and heat transport limitations still need to be improved.

Introduction

The past decade has witnessed growing scientific interest in the synthesis and use of carbon nanotubes for numerous potential applications which are the basis of the nanotechnology field.[1–5] In order to meet the potential applications which carbon nanomaterials are expected to fulfil, the problems of handling and structuring of these materials should be overcome. Indeed, carbon nanomaterials, *i.e.* nanotubes and nanofibers, are fluffy materials with an extremely high specific volume which render difficult their handling and transport. In addition, the nanoscopic shaping of these materials renders them unusable for fixed-bed catalytic processes due to the important pressure drop across the bed length. The macroscopic shaping of carbon nanotubes and/or carbon nanofibers has recently been reported by several groups in the literature in order to make these materials as competitive as the traditional supports for conventional chemical processes.[6–12] Another drawback of using carbon nanomaterials in catalytic processes is their high sensitivity to oxidation, and thus the catalytic applications are mainly confined to reductive atmospheres or to low temperature ranges in oxidative atmospheres in order to reduce the support loss by oxidation. Indeed, carbon nanofibers or nanotubes start to oxidize in air at temperatures above 500 °C and a significant loss of the material should be expected by surface or bulk combustion with a direct consequence of deteriorating catalyst body and activity. In addition, the presence of the active phase containing noble metals could significantly decrease the temperature of the support combustion which finally leads to loss of the catalytic performance. Therefore, it is of interest to find new composite materials with nanoscopic properties along with macroscopic shaping and high oxidative resistance in order to improve the materials' catalytic performance at high temperatures and oxidative atmospheres. The oxidative resistance of the support could also allow the oxidative regeneration of the catalyst, *i.e.* against coke poisoning, without problems encountered with the loss of support by surface combustion.

High thermal conductivity, high resistance towards oxidation, high mechanical strength and chemical inertness, properties required for use as heterogeneous catalyst supports, are exhibited by silicon carbide (SiC), and allow it to be a promising candidate to replace conventional industrial supports for several catalytic reactions.[13,14] The main drawback of SiC, synthesized by conventional high temperature processes, namely the very low specific surface area, *i.e.* close to 1 $m^2\ g^{-1}$, was overcome by the considerable attention focused on new preparative methods, allowing higher specific surface area SiC to be obtained in an industrial-like scale.[15–18] Today, the main catalytic research has been devoted to the use of silicon carbide in a macroscopic and traditional shape and size, *i.e.* extrudates, beads or foam, whereas the use of silicon carbide of a nanoscopic size is still scarce despite some recent scientific efforts devoted to the synthesis of SiC nanotubes, nanofibers and nanocables.[19–23]

It is noteworthy that all the methods reported up to now were devoted to the synthesis of nanoscopic SiC and no attention has been focused on the macroscopic shaping of these materials. Such an approach was very similar to that which happened with carbon nanotubes a decade ago. This renders them unusable for conventional applications, especially in catalysis, where the need for macroscopic shaping is increased. Indeed, as far as the literature results are concerned almost no studies dealing with the synthesis and use of nanostructured SiC composite with

[a]*Laboratoire des Matériaux, Surfaces et Procédés pour la Catalyse, UMR 7515 du CNRS, Université Louis Pasteur, European Laboratory of Catalysis and Surface Sciences (ELCASS), 25 rue Becquerel, 67087 Strasbourg, France. E-mail: cuong.lcmc@ecpm.u-strasbg.fr; Fax: (+) 33 3 90 24 26 74; Tel: (+) 33 3 90 24 26 76*
[b]*IPCMS—Groupe Surfaces et Interfaces, 23, rue du Loess, BP 43 F-67034 Strasbourg, France*
[c]*SiCAT SA, 1 rue du Broetsch, 67700 Otterswiller, France*
† Electronic supplementary information (ESI) available: Support; characterisation; and diesel particulate filtration. See DOI: 10.1039/b806785f

macroscopic shaping has been reported. It is though that SiC nanomaterials with high external surface areas, *i.e.* nanoscopic structures, and open porosity (absence of ink-bottled pores) could lead to new performance as structure bed catalysts by providing a higher accessibility of the reactants to the active sites and also to a high rate of product evacuation owing to the low diffusional distance.

Nowadays the eminent example of catalytic support used in the industry is a packed bed (spherical particles, extrudates and powder). However, packed beds induce important pressure drops at high flow, due to the low porosity (in the range 0.3–0.6). These problems encountered with conventional packings (spherical particles, extrudates, powder) could be overcome by using so called structured bed catalysts, *i.e.* foams, monoliths or even only coatings.[24] Amongst these different structured catalysts, solid foam represents the most appropriate material due to its open porosity, up to 95%.[25] This new foam material has a highly permeable porous structure with high porosity (0.6–0.95), which enables a considerable reduction of the pressure drop even at high gaseous space velocity. Moreover these porous structures present a high effective contact surface (m^{-1}) along with a relatively high specific surface area (*ca.* 50 m^2 g^{-1}) between the fluid and solid phases. Nowadays the ceramic-based (Al_2O_3, cordierite, SiC *etc.*) and metal based (aluminum, copper *etc.*) cellular foams are widely used in a large range of applications, especially employed in thermal applications.[26] Foam structures have also received more and more scientific and industrial interest as catalyst supports during the past decade, especially in catalytic processes which are limited by mass or heat transfer.[27,28] Thus, the main reasons why reticulated foams are so attractive in the catalysis field is their high effectiveness in heat and mass transfer properties, and a low pressure drop (large open porosity) combined with high specific surface area. However, foam structures have a relatively low surface interaction for performing good anchorage and dispersion of the active phase. In the case of this study, SiC foam presents a medium surface area [specific surface (10–20 m^2 g^{-1})] due to a natural wash-coat layer of SiO_2 and SiO_xC_y phases (but low compared to classical packing, *i.e.* extrudates). In this context, the addition of the nanometric size SiC nanorods or nanofibers presented in this work could significantly increase the surface interaction for subsequent better active phase dispersion while keeping the same hydrodynamic properties leading to more homogeneous mass and heat transfers with a low pressure drop. In addition, the nanometric size of the SiC nanorods or nanofibers could significantly decrease the mass transfer limitation which could modify in a great manner the overall activity and selectivity of the reaction when used in a fixed-bed reactor.

The aim of this study is to report for the first time the synthesis of SiC nanofibers with controlled macroscopic shape for several downstream applications including the catalysis and filtration domains. The as-synthesized SiC-based composite was characterised by several techniques including powder X-ray diffraction (XRD), scanning and transmission electron microscopy (SEM and TEM), pressure drop measurements and ^{29}Si MAS-NMR. The ability of the material to be used as an efficient filter in diesel particulate filtration, and especially for nanoparticle filtration, was also evaluated and presented.

Results and discussion

SiC composite synthesis

The SiC nanofibers supported on the macroscopic SiC host structure, *i.e.* foam, composite were synthesized in two steps: firstly a network of carbon nanofibers (CNFs) was grown on the SiC host structure by a catalytic CVD method and then the resulting CNFs/SiC composite was subsequently carburized with SiO vapour to form the final ceramic composite.

The SiC was obtained according to the gas–solid reaction[13,14,18] with an average pore (window) size of 1900 μm. The ceramic material was impregnated with an aqueous solution of $Ni(NO_3)_2$ with the theoretical loading set to 1 wt%. The solid was oven dried at 100 °C for 2 h and calcined in air at 350 °C for 2 h. The reduction was carried out *in situ* in flowing hydrogen at 400 °C for 2 h. After the reduction the hydrogen flow was replaced by a mixture of C_2H_6–H_2 (60/40 ml per minute) and the reaction temperature was increased from 400 to 680 °C (heating rate of 20 °C min^{-1}).[8] After synthesis over 4 h the reactor was cooled down to room temperature under the reactants' mixture. Before discharging, the reactor was flushed with helium flow for 30 min. The CNFs' yield was around 10 g of CNFs per g of Ni per hour at a synthesis temperature of 680 °C.

SiC nanofibers were synthesized by the reaction between the CNFs with the SiO vapours under an argon atmosphere at 1300 °C for 4 h in an electrical oven. The C-to-SiC transformation was accompanied by a consecutive release of CO which was actively flushed out from the reaction zone by argon flow, and thus shifting the reaction equilibrium towards the formation of SiC.[13] The relatively low synthesis temperature allows the conservation of the composite specific surface area unlike the high temperature synthesis where only very low specific surface area, *i.e.* 0.1 to 1 m^2 g^{-1}, α-SiC is obtained. After synthesis the composite was calcined in air at 600 °C for 2 h in order to remove the residual carbon from the matrix.

XRD and surface area characterisations

The efficiency of the carburization process and the crystallinity of the obtained materials were characterised by XRD as presented in Fig. 1. The residual carbon was further burned off by calcination in air at 700 °C for 2 h (heating rate of 5 °C min^{-1}). According to the XRD results the SiC is crystallised in a face centered cubic structure (fcc), β phase. However, some diffraction lines corresponding to the hexagonal phase were also observed. These diffraction lines were attributed to the presence of stacking faults along the growth axis (111), which induce a periodical hexagonal structure inside the material.[6,7] The stacking faults can be clearly visualised by the high resolution TEM micrograph of the material as presented in Fig. 5B.

The formation of the CNFs on the SiC foam surface induces a significant increase in the specific surface area of the pristine SiC host material from 10 to 60 m^2 g^{-1}. This significant improvement after the carbon nanofibers' deposition was directly attributed to the increase in the external surface area of the carbon material which provides an increase in the number of adsorption sites and thus leading to the surface area enhancement.[29,30] During the carburization process a slight decrease of the specific surface area was observed, 50 instead of 60 m^2 g^{-1},

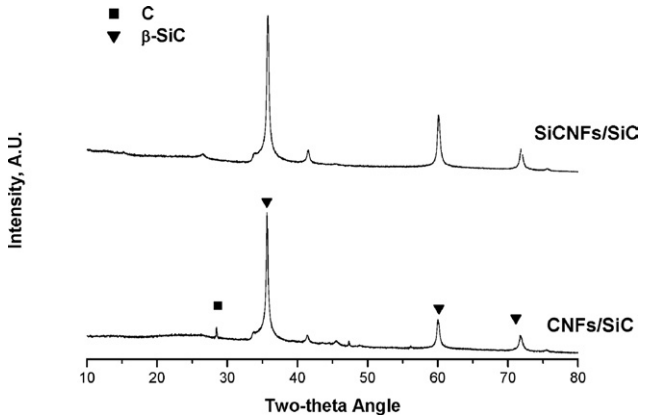

Fig. 1 XRD patterns of the CNFs/SiC foam and the same sample after carburization at 1250 °C. The residual carbon in the composite was removed by calcination at 700 °C in air for 2 h (heating rate of 5 °C min^{-1}).

which could be assigned to surface diffusion problems at high temperature and to the phenomenon of so called thickening of the SiC-based composite due to the presence of secondary synthesis reactions. The surface area loss by surface diffusion phenomena could be attributed to surface reorganisation at lower energy levels by filling or by collapsing of the pores. Similar results were reported by Elder and Krstic[31] and Hase *et al.*[32] in which it was observed that SiC started to sinter, by surface diffusion, at a temperature far lower than the theoretical sintering temperature. However, the sintering process was proportional to the surface energy of the material. The surface energy increases as the specific surface area of the material increases which is in a good agreement with the material processed in the present work. The thickening of the SiC nanofibers compared to the pristine carbon nanofibers could also originate from the specific surface area loss.

SEM morphology investigation

SEM micrographs of the CNFs/SiC foam composite are presented in Fig. 2A and show the presence of highly entangled carbon nanofiber structures with extremely high aspect ratios forming a dense web-like network on the surface of the SiC host structure. The as-synthesized fibers are well dispersed on the outer surface of the host matrix which confirms the high dispersion of the growth catalyst and high gaseous accessibility. It is noteworthy that the carbon nanofibers were strongly anchored on the ceramic macroscopic host structure as no weight loss was observed after sonication of the composite over 30 min. The high mechanical anchorage of the carbon nanofibers on the ceramic host structure could be explained by the nature of the fibers and their growth mechanism, *i.e.* an octopus-like growth process, which allows part of the formed carbon nanofibers to penetrate the host structure, and thus yielding a strong anchorage of the nanoscopic structure on the surface of the macroscopic support.

The as-synthesized CNFs/SiC foam composite was further carburized according to the gas–solid reaction,[13,14,33] for more details see the ESI†. Before carburization the sample was studied by TEM in order to ensure the nickel catalyst particles removal by means of acidic treatment. Statistical TEM analysis reveals that most of the CNFs growth Ni catalyst (1 wt%) was removed by the acidic treatment. However, some remaining nickel-based particles can be observed but they are completely encapsulated by the graphene layers during the cooling step of the synthesis and are no longer accessible for the further treatment steps. It is also noteworthy that during the carburization process the remaining Ni particles underwent transformations with SiO vapour and formed the $NiSi_2$ phase with no catalytic activity.

SEM micrographs of the SiC-NFs/SiC foam composite are presented in Fig. 3 with different magnifications. The low magnification SEM micrograph shows the complete conservation of the nanofibers' morphology when going from C to SiC. It could be underlined here the enormous advantage of the synthesis method for the hierarchical composite structure preservation with morphology conservation.

The high magnification SEM micrograph indicates that the SiC nanofibers were formed by a stacking of several SiC nanoparticles, with an average size of 50 to 70 nm along the fiber axis. The average diameter of the SiC nanowires is slightly increased when compared to the starting CNFs, *i.e.* 30–50 nm. Such an observation could be attributed to an epitaxial post-growth on the pristine surface of the SiC nanowires according to the following chemical reaction:

$$SiO\ (g) + 3\ CO\ (g) \rightarrow SiC\ (s) + 2\ CO_2\ (g)$$

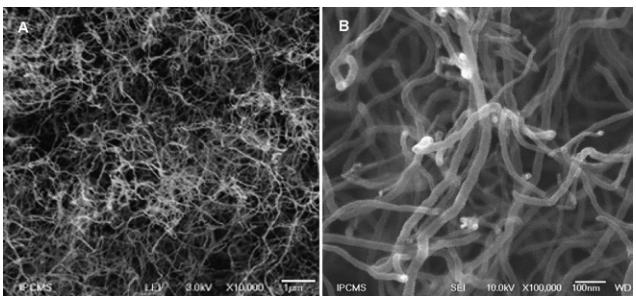

Fig. 2 (A, B) SEM micrographs with different magnifications showing the relative regular diameter of the as-synthesized carbon nanofibers. The CNFs have an average diameter centered between 30 to 50 nm and lengths of several tenths of micrometers.

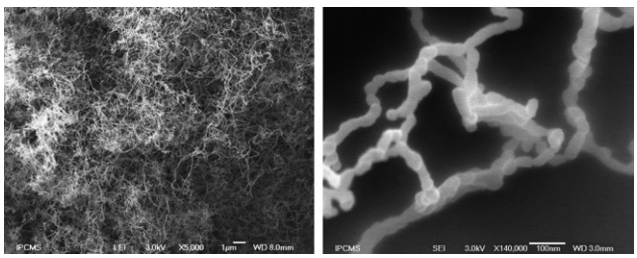

Fig. 3 SEM micrographs with different magnifications of the SiC-NFs/SiC foam composite synthesized by a gas–solid reaction between SiO vapours and CNFs at 1350 °C. The high magnification SEM micrograph indicates the presence of SiC nanoparticles stacked one on another along the fiber axis.

Similar observations have been already reported by Hu *et al.*[34] during the gas–solid reaction between the multi-walled carbon nanotubes and SiO vapour.

TEM characterisation

The TEM micrograph (Fig. 4A) of the as-synthesized CNFs indicates the formation of carbon nanofibers with a fish-bone microstructure and graphene planes very well graphitized and oriented with an angle of 75° along the fiber axis. However the existence of carbon nanofibers with bigger diameters, *i.e.* >40 nm, and graphene planes with less ordered structures could be observed (Fig. 4B). A thin layer of amorphous carbon is also formed on the surface of the nanofiber. Such amorphous carbon layers were expected to be created during the cooling step of the synthesis. Indeed, during the cooling step, the residual temperature was still high enough to decompose the gaseous hydrocarbon to atomic carbon but not high enough to allow the precipitation of ordered carbon structures. Similar results have already been reported by Ermakova *et al.*[35] during the synthesis of carbon nanotubes on the iron-based catalyst.

The microstructure of the SiC material was observed using a high resolution TEM technique and the corresponding images are presented in Fig. 5. The TEM study allows the determination of the microstructure relationship between the starting CNFs and the final β-SiC material. The TEM observations clearly indicate the modification of the CNFs microstructure after carburization. However the morphology, *i.e.* nanofibers' shape, remained similar in accordance with the SEM observations. Low magnification TEM micrographs show a similar microstructure between the starting CNFs and the final SiC, in the form of nanowires with curvature and highly entangled each others. However, at high resolution a large difference can be observed between the two materials. The relatively clean microstructure of the starting CNFs was no longer observed and the SiC nanofibers consisted of stacked SiC nanoparticles, *i.e.* nanochain structure, with an average diameter of around 50 nm (Fig. 5A). The formation of the SiC nanochains was expected to proceed in two steps. In the first step of the carburization process the SiC nanowires were formed by gas–solid reaction between the SiO vapour and the carbon nanofibers. As the reaction advances, an additional gas–gas growth of SiC onto these primary nanowires takes place and leads to the formation of a new superstructure, *i.e.* bead structure. Along the reaction the beads become bigger and bigger and, finally, lead to the formation of a SiC nanochain structure with high stacking faults along the (111) growth direction (Fig. 5B). Similar two-step growth mechanisms have been suggested by Wei *et al.*[36] and Hao *et al.*[37] to explain the formation of SiC nanochains with a periodically beaded superstructure. However a different morphology of the SiC, *i.e.* periodical beads instead of nanochains, in this work has been observed compared to the reported works[36,37] and could be explained principally by the difference in the synthesis conditions.

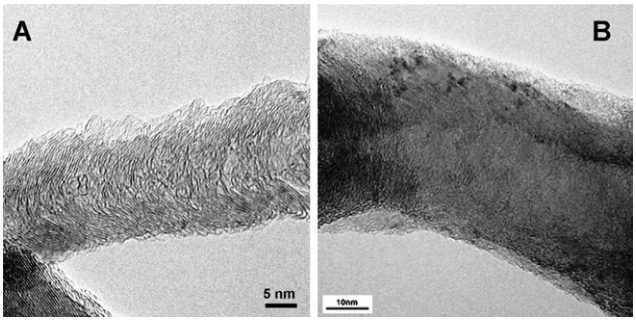

Fig. 4 (A,B) TEM micrographs of the carbon nanofibers formed on the macroscopic SiC host structure before further carburization. The high resolution SEM micrograph provides evidence of the fish-bone microstructure of the carbon nanofiber with prismatic planes exposure.

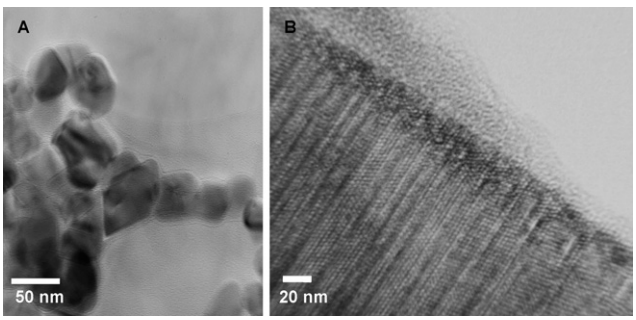

Fig. 5 (A) Low magnification TEM image of SiC nanofibers formed by stacked SiC nanoparticles. Statistical TEM observations reveal the slight increase of the average diameter of the nanofiber from C-to-SiC. (B) High resolution TEM image of the SiC nanofiber showing the presence of a high stacking faults density along the (111) growth axis which is responsible for the diffraction lines corresponding to the side hexagonal phase in the material.

It is significant to mention that along with the SiC nanochains some SiC nanowires were also observed in the composite (Fig. 6A). High resolution TEM observations clearly show the right orientation of the SiC planes along the (111) direction (Fig. 6B).

The vapour–liquid–solid (VLS) mechanism[38] cannot be taken into account in the present work in which, if such a mechanism is operating, one should expect to find a solid catalyst on the top of the whisker. TEM observations carried out on different samples have not shown evidence of such a solid on the top of the SiC-based material. A work published previously has shown that the SiC formation was limited by the SiO concentration in the reaction medium.[39] The observed mechanism belongs to the shrinking core model (SCM) which has been developed by Hurst *et al.*[40] and by Falconer and Schwartz[41] for oxide materials reduction. When such a mechanism is followed, the reactive surface at the beginning of the reaction offers higher surface area

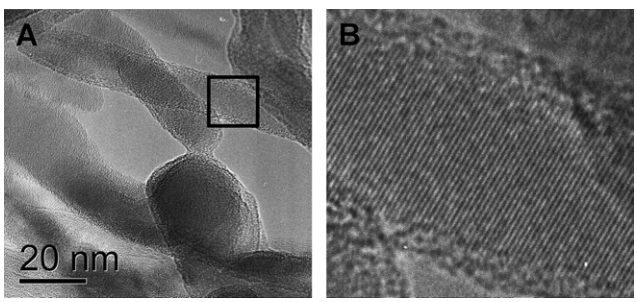

Fig. 6 (A, B) High resolution TEM images of the SiC nanofibers.

and then, continuously shrinks with the progressive coverage of carbon nanofibers by SiC, thus limitting the diffusion of SiO and CO in and out of the material.

It is noteworthy that the as-synthesized SiC nanobeads do not exhibit an empty porosity at the center observed for the traditional SiC material. This could be explained by the fact that the SiC nanobeads are formed by slowly shrinking the bear central porosity to yield the bulk material. Such shrinkage could be partly responsible as well for the loss of the specific surface area after the carburization process.

The high resolution TEM image also gives evidence of the presence of a large number of stacking faults along the growth axis [111] of the SiC. The preferential growth of SiC along the [111] direction is due to the lowest surface energy of the (111) plane. The structure of SiC is based on the stacking of close packed layers of silicon and carbon atoms along the [111] or [0001] direction utilizing corner-sharing SiC tedrahedra resulting in a regular 3-layer repeat sequence ABCABC… The stacking sequences sometimes may break the periodicities, resulting in stacking faults. SiC generally contains stacking faults along the [111] direction. The high number of stacking faults observed in our sample was attributed to the low synthesis temperature which favours the misalignment sequence along the growth axis.[6,7]

The TEM micrograph also reveals that the SiC nanofibers were constituted of several SiC nanoparticles with different crystalline orientations. All the different orientations within the SiC nanofibers were attributed to the simultaneous formation of several nucleus sites during the carburization process leading to the generation of polycrystalline SiC nanoparticles. TEM observation indicates that the surface of the SiC nanofibers was covered by a thin amorphous layer at *ca.* 2–3 nm (Fig. 5B). This amorphous layer was expected to be formed when the sample comes into contact with air according to the high sensitivity of the SiC surface to oxygen even at room temperature. XPS analysis reveals that this amorphous phase was constituted of a mixture of SiO_2 and SiO_xC_y. The oxygen-containing layer will play a role in natural wash-coating during the deposition of the catalytically active phase onto the ceramic surface.[18] Indeed, it has been observed that the catalytic active phase, *i.e.* metal, oxide or sulfide, deposited on SiC surface exhibits a relatively high degree of dispersion even despite of the chemical inertness of the ceramic support.[14] Such a high dispersion was attributed to the existence of peculiar metal–support interactions which led to the formation of discrete nanoparticles on the support surface despite the chemical inertness of the support.

Pressure drop experiments

Pressure drop is a very important parameter for the characterisation of catalytic supports employed in industrial applications. In fact the knowledge of the pressure drop induced by the support is essential for successful design and high performance of the industrial systems, especially in the case of high space velocity applications where the pressure drop problem could be detrimental to the safety and performance of the operating unit. The introduction of the nanoscopic material into the macroscopic host matrix generally will develop a pressure drop due to the open space narrowing through the composite. From this point of view the measurements of the pressure drop with and without the nanofibers are necessary and will be studied and discussed below.

Table 1 Influence of the support morphology on the composite characteristics, BET surface area and the effective surface area

Characteristics of support	SiC extrudates	SiC foam	SiC foam with 5% SiCNFs	SiC foam with 39% SiCNFs
Cell diameter		1900 μm	1900 μm	1900 μm
Apparent mass, ρ_{app}	770 g l^{-1}	103 g l^{-1}	107.5 g l^{-1}	169 g l^{-1}
Open porosity, ε	0.38	0.94	0.937	0.902
Strut diameter or equivalent strut diameter	3 mm	157 μm	161 μm	211 μm
Specific surface area, ac_g	1461 m^{-1}	1530 m^{-1}	1560 m^{-1}	1852 m^{-1}
Specific surface interaction, BET	34 m^2 g^{-1}	10 m^2 g^{-1}	19 m^2 g^{-1}	50 $m^2.g^{-1}$

The experimental setup used has already been presented in a previous work.[42] The reactor (I.D. = 25.4 mm) was packed with 3 mm SiC extrudates particles or SiC foam with or without nanofibers to have a total bed height of 4 cm (see Table 1 for the main characteristics of each bed). The facility is maintained in a hermetic regime to prevent any gas leaks. The single-phase (air flow) pressure drop is measured across the whole packed bed section with differential pressure sensors and the results are presented in Fig. 7.

The results show that in the case of extrudate beds, the pressure drop is important at low space velocities and becomes even larger when the gas velocity increases. At high gas velocities, for example 3 m s^{-1}, the pressure drop was near 1×10^4 Pa m^{-1} for the foam, whereas it was 9 times higher for the extrudate beds. Richardson *et al.*[43] have observed similar results and quote a factor of 10 between the pressure drop of the foam type supports and spherical particle fixed-beds. When the SiC

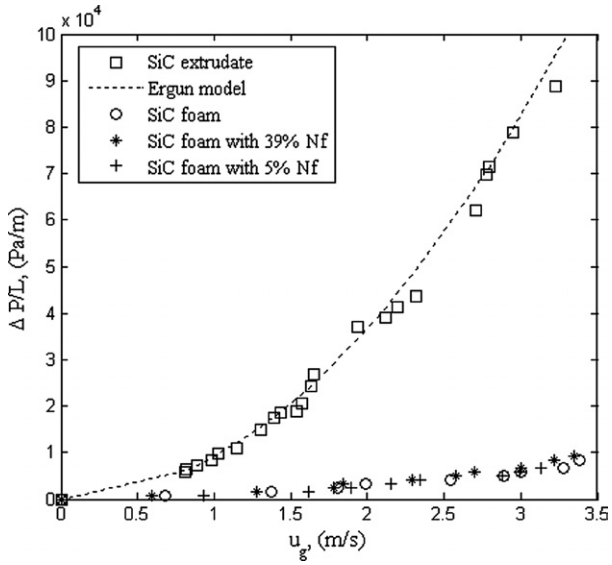

Fig. 7 Pressure drop as a function of linear gas space velocity of the bare SiC foam, extrudates and the SiC-NFs/SiC foam composites with different amounts of nanofibers.

nanofibers are applied the specific surface area increases but the pressure drop remains unchanged. This result clearly shows that even with a high effective specific surface area (value derived from the BET measurements shown in Table 1), the pressure drop through the SiC-NFs/SiC foams is lower than that observed for the packed bed of extrudates. This result confirms the preliminary statement that the nanofibers supported on foam host structure are good candidates for use as a supports in catalytic applications with short contact times (*i.e.* high reactant flows).

The introduction of the nanoscopic properties onto the macroscopic host matrix hardly influences the pressure drop, as shown in Fig. 7. To explain this phenomenon, the pressure drop on the SiC-NFs/SiC foam composite has been estimated by the cubic cell model developed previously in the laboratory[42] which gives a good agreement between estimated pressure drops and experimental data. In the pressure drop simulations, cell diameter is constant and only foam apparent density and, as a consequence, porosity change. As seen from Table 1, the porosity hardly decreases with the nanofibers' deposition. The calculated equivalent strut diameter increases and, as estimated by Ergun's equation, only a low enhancement of the pressure drop is induced.

To clarify the influence of the nanofibers' deposition on the bare strut diameter microscopic observations have been carried out. The SEM image (Fig. 3) shows a complete coverage of the SiC foam surface by a dense web network constituted of entangled SiC nanofibers. Thus for modeling the pressure drop (Fig. 8) on foam covered by nanofibers, it is sufficient as a first approximation to consider that the nanofibers are homogeneously distributed and increase the apparent strut diameter.

As seen from the figure the approach is well adapted to the experimental data and permits a better future process design only with simple knowledge of the apparent density (and thus porosity) to estimate the pressure drop.

The most important conclusion that comes out from this pressure drop study is that the introduction of SiC nanofibers allows a significant improvement in the overall BET specific surface area and effective surface area of the solid without introducing an additional pressure drop which could be detrimental for the low contact time reactions.

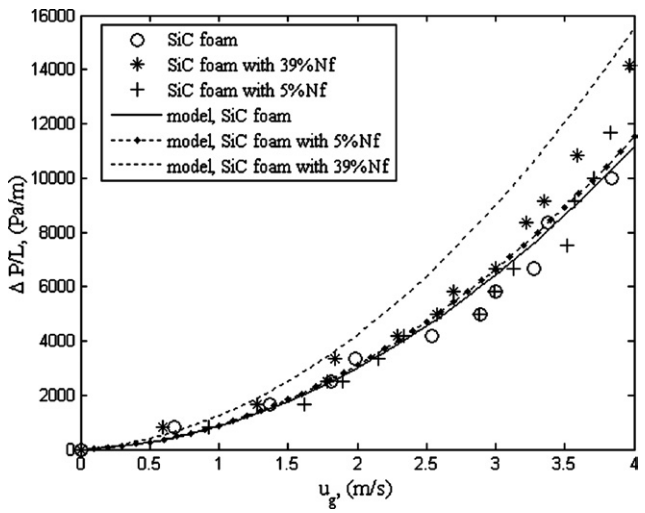

Fig. 8 Experimental data and simulated pressure drop results comparing the starting SiC foam and the SiC-NFs/SiC foam composite as a function of linear space velocity.

Mechanical anchorage

Another important characteristic of the present ceramic composite is the mechanical stability and the degree of anchorage of the nanofibers on the host matrix. The dust formation during preparation and especially application is an important factor that should be taken into account as such phenomenon could give rise to material loss with time on stream and as a consequence, the loss of the overall efficiency of the system.

The mechanical anchorage of the nanofibers on the SiC foam surface was checked by submitting the sample to a sonication treatment for 30 min in an ethanolic solution. According to the results no SiC nanofiber loss was observed after the sonication treatment demonstrating the high mechanical anchorage of the carbon nanofibers on the SiC foam host structure. Previous results have shown that the carbon nanofibers were formed *via* an octopus-like growth mechanism from a single nickel catalyst particle.[44] It is expected that part of carbon nanofibers are deeply infiltrated in the SiC matrix, and thus lead to stronger anchorage of the nanomaterial network to the SiC host structure. As a confirmation of this hypothesis the synthesis duration has been increased resulting in a higher number of carbon nanofibers. At higher carbon nanofibers numbers the macroscopic ceramic host structure is made fragile and results in complete destruction of the shape at the end of the synthesis. The shape destruction is attributed to the deep penetration of the formed carbon nanofibers, which leads to the dislocation of the macroscopic structure and, as a consequence, the loss of this later by grain boundary breaking. Similar results have already been reported by other authors in the literature where carbon nanofiber formation could lead to the destruction of a reactor walls.[45]

Oxidative resistance improvement by C-to-SiC transformation

The oxidative resistance is an important drawback for carbon-based materials which needs to be improved or solved in order to allow the effective use of these composite materials in an aggressive environments, *i.e.* high temperature and oxidative atmospheres. The improvement of the oxidative resistance of the material when going from CNFs/SiC to SiC-NFs/SiC (C-to-SiC) was studied by Temperature-Programmed Oxidation (TPO)† and the results are presented in Fig. 9A. The C-to-SiC transformation allows a significant increase in the oxidation temperature from 550 to 700 °C. SiC is well known to possess a higher oxidative resistance compared to carbon-based materials and starts to oxidize at 700 °C. In addition, during the oxidation SiC also developps a oxidized surface layer which protects it against further oxidation. Indeed, the first layers of SiO_2 formed on the SiC surface play a role of diffusion barrier and thus, prevents or slows the oxygen diffusion into the ceramic bulk matrix according to the core shrinking model.[46] From these results, one should note that despite the very similar specific surface, the final nano–macro shaped ceramic composite is far more resistant to oxidative treatement which renders it an interesting

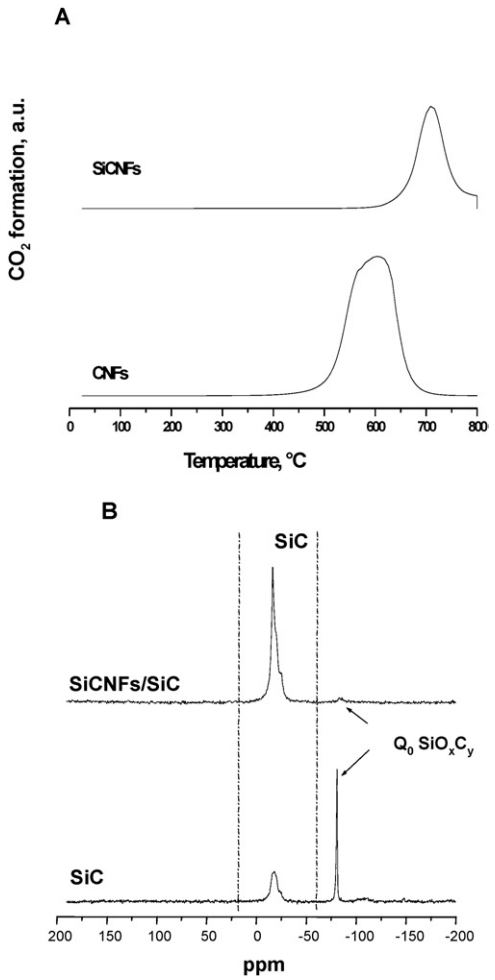

Fig. 9 (A) TPO spectra of the CNFs/SiC and SiC-NFs/SiC composites showing a significant improvement in terms of the oxidative resistance of the ceramic-based composite. (B) ^{29}Si NMR spectra of the pristine SiC foam and the SiC-NFs/SiC composite showing a significant reduction in SiO_2 formation on the composite after oxidative thermal treatment.

candidate for use as a catalyst support in high temperature reactions under oxidative atmospheres.

Oxidative resistance improvement by nanostructured ceramic addition

The deposition of a network of SiC nanofibers on the SiC foam structure also significantly improves the oxidative resistance of the ceramic material compared to the pristine SiC support under similar oxidative conditions. The oxidative resistance of the SiC-based composites was studied by ^{29}Si MAS-NMR in order to give access to the chemical environment and the geometry of the silicon engaged inside the ceramic structure (Fig. 9B). The ^{29}Si NMR spectrum of the ceramic composite was compared to that of the bare SiC foam support. Both samples have been preliminarily treated at 900 °C for 2 h in air. According to the results one should state that the introduction of the SiC nanofibers onto the pristine SiC foam surface led to a significant reduction of the surface oxidation testified by the ^{29}Si peak at −80 ppm attributed to SiO_2 and/or SiO_xC_y layer[47] on the pristine SiC surface. Up to now, the improvement of the SiC-based composite in terms of oxidative resistance compared to the pristine host matrix was not well understood. An additional study using high resolution TEM technique coupled with EELS is in progress in order to clarify this point.

The carbon and oxygen concentration on the two forms of SiC, *i.e.* SiC and NF-SiC/SiC, are investigated by means of XPS technique and the results are presented in Fig. 10. The XPS results clearly give evidence of the significant reduction of the Si–O surface contribution on the NF-SiC/SiC compared to that observed on the pristine support and confirms NMR results about the higher oxidative resistance of the NF-SiC-based material.

The following hypothesis could be proposed to explain the observed results: the homogeneous growth of the SiC nanofibers modifies the microstructure of the pristine SiC host, thus modifing the oxygen adsorption and/or diffusion and finaly resulting in the oxidation of the composite. The microstructures of the SiC beads inside the nanofibers could also modify the oxidative behavior of the material. Work is on going in order to get more insight about the high oxidative resistance of the SiC-based composite.

The nano–macro composite C-NFs/SiC and SiC-NFs/SiC can be synthesized in different shapes, *i.e.* grains, extrudates, beads, foam with different pore openings and structures depending on the downstream applications. Some examples of these

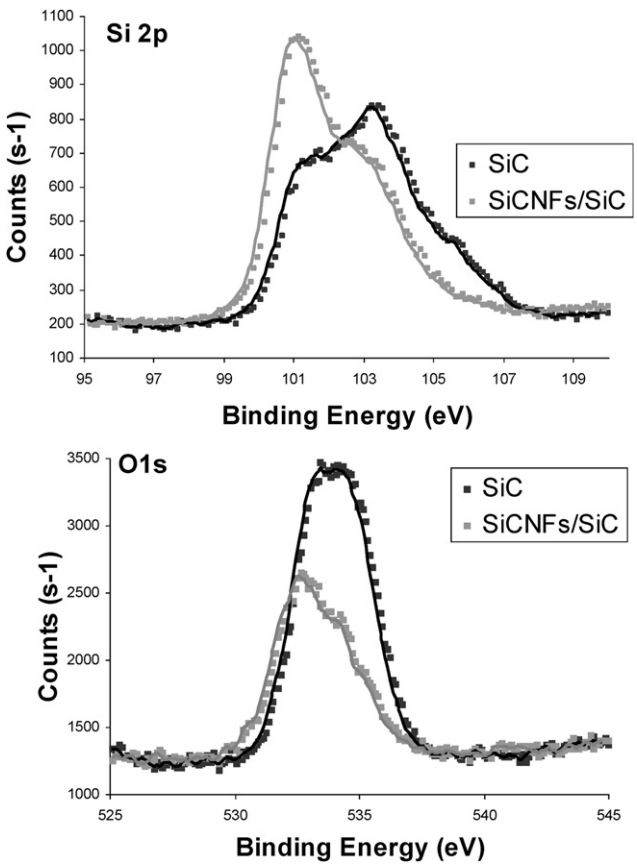

Fig. 10 XPS spectra of Si_{2p} and O_{1s} recorded on the SiC foam and the NF-SiC/SiC foam which evidences the lower degree of surface oxidation in the presence of nanofiber ceramic.

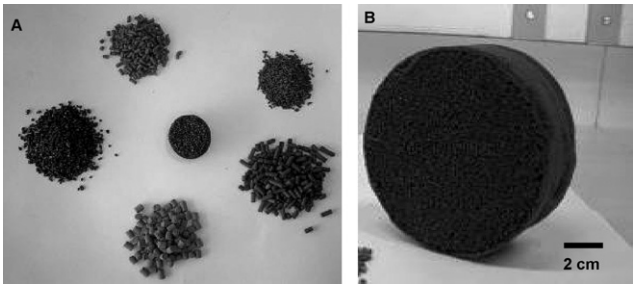

Fig. 11 (A, B) Macroscopic sizes and shapes of different SiC nanofiber composites, *i.e.* foams, extrudates, grains.

composites are presented in Fig. 11A. The carbon nanofibers' growth rate hardly changes as a function of the SiC macroscopic shapes. This result is attributed to the absence of micropores which could induce diffusion into the SiC host structure. By tuning the synthesis duration one can efficiently control the final surface area of the C-NFs/SiC composite from 50 to more than 150 m^2 g^{-1} depending on the downstream applications. Such carbon-ceramic composite can be directly employed as a support for low temperature liquid and gas-phase reactions or to be carburized for high temperature oxidative reaction applications.

The macroscopic shape of the materials can be controlled on a large range, from centimetre size to several dozen centimetres in size or even more, depending on the downstream application. It is noteworthy that the SiC nano–macro composites can be tailored even after synthesis to obtain the desired shape for the downstream reactions. For example, a macroscopic piece of the foam-based ceramic composite with a diameter up to 100 mm and length of 500 mm can be synthesized for subsequent use in diesel particles filter devices (Fig. 11B).

All the samples were synthesized by a gas–solid reaction between the composite carbon nanofibers/SiC host structure and the SiO vapour at 1300 °C in flowing argon.

Diesel particulate filtration

The SiC-NFs/SiC foam composite was further integrated in a bench test as a filter for diesel particulates. Fibrous aerosol filters allow the particulates' interception by a combination of several means, *i.e.* available filter surface, inertial particle impact on the filter surface, Brownian diffusion of particles inside the filter, porosity and the particulate size inside the aerosol. The diameter of the fiber which constituted the filter plays an important role in the filtration efficiency according to the work reported by Viswanathan *et al.*[48] The experimental setup is described in detail in the ESI.† The filtration efficiency of the SiC-NFs/SiC foam composite is presented in Fig. 12. According to the results the filtration efficiency, especially for the small soot particles, *i.e.* < 0.2 μm, was significantly improved in the case of the nano–macroscopic composite compared to that of the SiC foam. The high filtration efficiency for small particulates is attributed to the high surface contact between the filter, *i.e.* high effective surface area and tortuosity, and the aerosol passing through, which significantly improve the particles interception. The high efficiency of the ceramic composite filter for nanoparticle filtration is an extremely important fact as generally

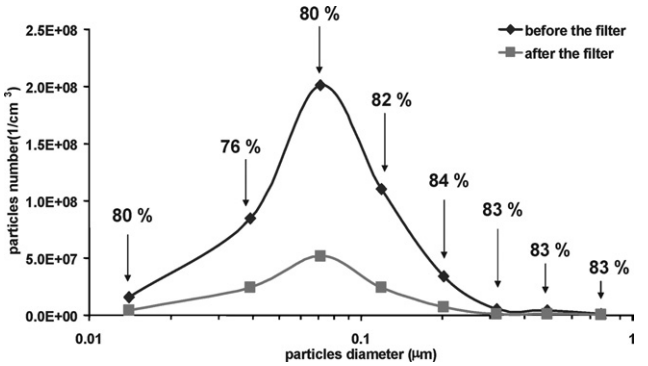

Fig. 12 Filtration efficiency of the diesel particulates (DPs) issued from a diesel car engine (for details see the ESI†). The space velocity was fixed at 250 000 h^{-1} (linear velocity 5 m s^{-1}). The filter was constituted of a cylinder of SiC foam (45 ppi) with a length of 50 mm and a diameter of 100 mm.

traditional filters fail to retain nanoparticles. Such nanoparticle filtration efficiency can be effectively transmitted to gasoline engines where the main part of the emitted particles are in the nanoscopic range. According to the literature results, the filtration efficiency increases as a function of the filter thickness and the diameter of the fibers which constitute the filter.[49] The open porosity of the filter, due to the combination of a macroscopic structure and nanoscopic material coated on the external surface, can also lead to a very small pressure drop during the filtration step according to the differential pressure measured at the entrance and exit of the filter despite the relatively high gaseous linear velocity.

Conclusions

In summary, it is the first time that the direct synthesis of SiC nanostructures with direct macroscopic shaping has been reported. The present method allows a rapid and complete coverage of the macroscopic SiC foam by a dense and homogeneous network of carbon nanofibers which were further transformed into the corresponding SiC nanofibers. The introduction of the network of carbon nanofibers onto the SiC foam host structure led to a significant increase in the overall specific surface area of the final CNFs/SiC composite, from 10 to 60 m^2 g^{-1}. After carburization, a slight decrease in the specific surface area is observed, 50 instead of 60 m^2 g^{-1}, essentially due to surface diffusion at high temperature and also to the thickening of the final SiC nanofibers due to the dual growth mechanism. It is noteworthy that the specific surface area obtained in the present work is the highest ever obtained for macroscopic shaped ceramics. It is very important to insist that the current method of preparation could open the door to a wide variety of composite supports with dual properties, *i.e.* nanoscopic surface properties combined with controlled macroscopic shaping, which could find useful application as a catalyst support in the field of heterogeneous catalysis as well as in the field of nanomaterial filtration.

A simple pressure drop model using the standard Ergun's equation and based on a cubic lattice approach for the foam structure is used. This model allows the prediction of

experimental data on the foam structure with or without nanofibers. The experimental data and calculated pressure drops show that the introduction of the nanoscopic material into the macroscopic host matrix hardly has an influence on the pressure drop in spite of the dramatic improvement of the effective surface area of the composite.

The as-synthesized ceramic composite supports can be also doped before carburization with various elements which strongly modify either the chemical properties of the support or its intrinsic specific surface area depending to the reactions. The catalytic evaluation of this new nano–macroscopic support will be conducted with methane reforming as an example of a reaction in high oxidative media and with high mass and heat transfer limitations.

Finally, the high efficiency of the nano–macro ceramic composite as a filter for fine and ultrafine soot particles holds great promise for developing of the new filtration systems, especially for ultrafine particle retention as in the case of a gasoline exhaust engine. These nano–macro ceramic composites can also be effectively employed as filters for the capture of microorganisms such as viruses. The possibility of selective grafting of photocatalysts oto such composite surfaces could also open the door for direct destruction of viruses by capture followed by UV-light irradiation or by thermal treatment. It is also noteworthy that the high thermal resistance of the ceramic composite allows it to be employed as a filter in an aggressive media such as high temperature and/or acidic or basic environments.

Acknowledgements

The present work is financially supported by Sicat SA Otterswiller, France. Dr Th. Dintzer (LMSPC) is gratefully acknowledged for performing SEM experiments. P. Bernhardt (LMSPC) is also gratefully acknowledged for performing XPS analysis. Dr S. Rigolet and Dr Cl. Marichal (LCPM) are gratefully acknowledged for performing ^{29}Si NMR analysis and for helpful discussion.

References

1 *Carbon Nanotubes: Preparation and Properties*, ed. T. W. Ebbesen, CRC Press, Boca Raton, 1997.
2 P. M. Ayajan, *Chem. Rev.*, 1999, **99**, 1787.
3 K. P. de Jong and J. W. Geus, *Catal. Rev. Sci. Eng.*, 2000, **42**, 481.
4 J. M. Nhut, R. Vieira, L. Pesant, J. P. Tessonnier, N. Keller, G. Ehret, C. Pham-Huu and M. J. Ledoux, *Catal. Today*, 2002, **76**, 11.
5 C. N. R. Rao and A. Govindaraj, *Nanomaterial Synthesis*, RSC, Cambridge, 2005.
6 N. A. Jarrah, J. G. van Ommen and L. Lefferts, *Catal. Today*, 2003, **79–80**, 29.
7 N. A. Jarrah, J. G. van Ommen and L. Lefferts, *J. Mater. Chem.*, 2004, **14**, 1590.
8 R. Vieira, M. J. Ledoux and C. Pham-Huu, *Appl. Catal., A: Gen.*, 2004, **274**, 1.
9 S. Rul, C. Laurent, A. Peingney and A. Rousset, *J. Eur. Ceram. Soc.*, 2003, **23**, 1233.
10 E. Ochoa-Fernandez, D. Chen, Z. Yu, B. Totdal, M. Ronning and A. Holmen, *Catal. Today*, 2005, **102–103**, 45.
11 P. Li, T. Li, J. H. Zhou, Z.-J. Sui, Y.-C. Dai, W.-K. Yuan and D. Chen, *Microporous Mesoporous Mater.*, 2006, **95**, 1.
12 E. Garcia-Bordeje, I. Kvande, D. Chen and M. Ronning, *Adv. Mater.*, 2006, **18**, 1589.
13 M. J. Ledoux, J. Guille, S. Hantzer and D. Dubots, US Pat., 4 914 070, 1990.
14 M. J. Ledoux and C. Pham-Huu, *Catal. Today*, 1992, **15**, 263.
15 M. A. Vannice, Y. L. Chao and R. M. Friedman, *Appl. Catal.*, 1986, **20**, 91.
16 P. W. Lednor, *Catal. Today*, 1992, **15**, 243.
17 R. Moene, H. T. Boon, J. Schooman, M. Makkee and J. A. Moulijn, *Carbon*, 1996, **34**, 567.
18 M. J. Ledoux and C. Pham-Huu, *CATTECH*, 2002, **4**, 226.
19 G. Gundiah, G. Madhav, A. Govindaraj, M. Seikh and C. N. R. Rao, *J. Mater. Chem.*, 2002, **12**, 1606.
20 C. Pham-Huu, N. Keller, G. Ehret and M. J. Ledoux, *J. Catal.*, 2001, **200**, 400.
21 V. Raman, G. Bhatia, S. Bhardwaj, A. K. Srivastava and K. N. Sood, *J. Mater. Sci.*, 2005, **40**, 1521.
22 H. F. Zhang, C. M. Wang and L. S. Wang, *Nano Lett.*, 2002, **2**, 941.
23 Y. J. Hao, J. B. Wagner, D. S. Su, G. Q. Jin and X. Y. Guo, *Nanotechnology*, 2006, **17**, 2870.
24 A. Cybulski and J. A. Moulijn, *Structured Catalysts and Reactors*, Marcel Dekker, New York, NY, 1998.
25 J. Banhart, *Prog. Mater. Sci.*, 2001, **46**, 559.
26 T. J. Lu, H. A. Stone and M. F. Ashby, *Acta Mater.*, 1998, **46**, 3619.
27 J. T. Richardson, D. Remue and J. K. Hung, *Appl. Catal., A: Gen.*, 2003, **250**, 319.
28 L. Giani, G. Groopi and E. Tronconi, *Ind. Eng. Chem. Res.*, 2005, **44**, 4993.
29 Y. J. Hao, G. Q. Jin, X. D. Han and X. Y. Guo, *Mater. Lett.*, 2006, **60**, 1334.
30 V. Raman, G. Bhatia, A. K. Mishra, S. Bhardwaj and K. N. Sood, *Mater. Lett.*, 2006, **60**, 3906.
31 P. Elder and V. D. Krstic, *J. Mater. Sci. Lett.*, 1989, **8**, 941.
32 T. Hase, B. W. Lin, T. Iseki and H. Suzuki, *J. Mater. Sci. Lett.*, 1986, **5**, 69.
33 M. J. Ledoux, S. Hantzer, C. Pham Huu, J. Guille and M.-P. Desaneaux, *J. Catal.*, 1988, **114**, 176.
34 L. Hu, Y. X. Li, X. X. Ding, C. Tang and S. R. Qi, *Chem. Phys. Lett.*, 2004, **397**, 271.
35 M. A. Ermakova, D. Yu. Ermakov, A. L. Chuvilin and Gennady G. Kuvshinov, *J. Catal.*, 2001, **201**, 183.
36 J. Wei, K. Z. Li, H. J. Li, Q. G. Fu and L. Zhang, *Mater. Chem. Phys.*, 2005, **95**, 140.
37 Y. J. Hao, J. B. Wagner, D. S. Su, G. Q. Jin and X. Y. Guo, *Nanotechnology*, 2006, **17**, 2870.
38 E. I. Givarginov, *J. Cryst. Growth*, 1975, **31**, 20.
39 N. Keller, C. Pham-Huu, S. Roy, M. J. Ledoux, C. Estournès and J. Guille, *J. Mater. Sci.*, 1999, **34**, 3189.
40 N. W. Hurst, S. J. Gentry, A. Jones and B. D. McNicol, *Catal. Rev. Sci. Eng.*, 1982, **24**, 233.
41 J. L. Falconer and K. A. Schwartz, *Catal. Rev. Sci. Eng.*, 1983, **25**, 141.
42 M. Lacroix, P. Nguyen, D. Schweich, C. Pham Huu, S. Savin-Poncet and D. Edouard, *Chem. Eng. Sci.*, 2007, **62**, 3259.
43 J. T. Richardson, Y. Peng and D. Remue, *Appl. Catal., A: Gen.*, 2000, **204**, 19.
44 C. Pham-Huu, R. Vieira, B. Louis, A. Carvalho, J. Amadou, T. Dintzer and M. J. Ledoux, *J. Catal.*, 2006, **240**, 194.
45 M. S. Hoogenraad, PhD thesis, Utrecht University, 1995.
46 S. Yagi and D. Kunii, in *Fifth Symposium (International) on Combustion*, Reinhold, New York, 1955, p. 231.
47 K. Guerfi, S. Lagerge, M. J. Meziani, Y. Nedellec and G. Chauveteau, *Thermochim. Acta*, 2005, **434**, 140.
48 G. Viswanathan, D. B. Kane and P. J. Lipowicz, *Adv. Mater.*, 2004, **16**, 2045.
49 *Aerosol Technology*, ed. W. C. Hinds, Wiley-Interscience, New York 1999.

